Journal of Fluids and Structures 54 (2015) 701–718

Contents lists available at ScienceDirect

Journal of Fluids and Structures

journal homepage: www.elsevier.com/locate/jfs

Post-critical analysis of highly deformable Joined Wings: The concept of snap-divergence as a characterization of the instability

L. Demasi [a,*], R. Cavallaro [a,b], F. Bertuccelli [a,c]

[a] Department of Aerospace Engineering, San Diego State University, United States
[b] Department of Structural Engineering, University of California, San Diego, United States
[c] Dipartimento di Ingegneria Aerospaziale, Università di Pisa, Italy

ARTICLE INFO

Article history:
Received 31 October 2013
Accepted 19 January 2015
Available online 18 February 2015

Keywords:
Joined Wings
Snap divergence
Post-critical analysis
Instability
Geometric nonlinearity
Sensorcraft

ABSTRACT

Theoretical modeling of the aeroelastic static instability with the possibility of tracing post-critical branches (via arc length technique) in the framework of Joined Wings has never been presented before. A complete formulation of the numerical iterative method of solution of the aeroelastic equations is presented.

The true critical condition is compared with the divergence speed evaluated by solving an eigenvalue problem about a steady state equilibrium, showing how this last approach may be unreliable and even nonconservative.

This work also explores the theoretical implications of using mechanical loads to mimic the real loading conditions.

A physical interpretation based on the aeroelastic effects, overconstrained nature of the system, and the bending/torsion coupling, is provided to interpret the conditions that lead to the snap-divergence.

1. Introduction

Typical joined-wing configurations (Wolkovitch, 1986; Chambers, 2005) are characterized by significant structural geometric nonlinearities (Blair et al., 2005; Kim et al., 2008; Liu et al., 2010). As a consequence, preliminary design complexity is increased (Blair et al., 2005): existing procedures successfully adopted by the aerospace industry rely mainly on linear tools not able to correctly reproduce these effects. Employment of these lower fidelity tools is actually a practical requirement since a Multi-Disciplinary Optimization (MDO) generally involves a large amount of analyses.

What has proven to be very effective in the past for classical cantilevered configurations, then, cannot (Kim et al., 2008) be directly translated into procedures that have the same degree of computational efficiency and accuracy, when Joined Wings are considered (Weisshaar and Lee, 2002).

On the other hand, neglecting structural nonlinearities in the early design stages may lead to a posteriori-verified unacceptable solutions and can determine a significant increase of design costs.

In this scenario, reduced order models specifically tailored to retain the important nonlinearities of Joined Wings can be an ideal solution. Unfortunately, even advanced reduced order modeling techniques proved not to be very effective (see Demasi and Livne, 2007; Demasi and Palacios, 2010; Phlipot et al., 2014; Teunisse et al., 2014) when Joined Wings were

* Corresponding author.
E-mail address: ldemasi@mail.sdsu.edu (L. Demasi).

http://dx.doi.org/10.1016/j.jfluidstructs.2015.01.009
0889-9746/

considered. This suggests taking one step back and focusing on the nature of the involved nonlinearities, with the final goal of capturing the essential underlying physics for a more accurate and efficient design of reduced order models.

Several efforts considered mechanical loading and showed a highly complex nonlinear behavior of Joined Wings. Besides numerical approach, also experimental work (Kim et al., 2011; Boston et al., 2010) was carried out to explore the joined-wing Sensocraft (Reichenbach et al., 2011; Scott et al., 2011; Heeg and Morelli, 2011) response when subjected to follower static loads. Different works discussed theoretical aspects related to the structural nonlinearities (Sotoudeh and Hodges, 2011) and also involved aeroelastic investigations (Patil, 2003; Demasi and Livne, 2005, 2009b; Cavallaro et al., 2014b).

Only recently (see Demasi et al., 2013b; Cavallaro et al., 2012, 2014a, 2014c), the research moved on the fundamental understanding of the peculiar nonlinear response of Joined Wings, with focus on the so-called *PrandtlPlane* configurations (e.g., Frediani, 1999, 2002, 2003, 2005; Frediani et al., 2012).

In particular, Demasi et al. (2013b) demonstrated via nonlinear investigations that the linear buckling analysis is not very reliable as far as the static critical condition is concerned. Moreover, the wing system might be sensitive to snap-buckling type of instability for some combinations of structural parameters. The so-called Snap-Buckling Region (SBR) for Joined Wings was then introduced. Load repartition between the wings, joint size, and sweep angle had an important impact on the stability properties.

Cavallaro et al. (2012, 2014a) presented several counter-intuitive aspects. Stiffening the compressed upper wing actually decreased the critical load; in addition, the lower-to-upper-wing bending stiffness ratio was shown to be one of the major parameters ruling the snap-buckling phenomenon. One of the most important physical aspects was the bending moment transferring through the joint: a reduction of the amount of transferred bending moment, obtained by changing the boundary conditions at the joint, significantly reduced the risk of snap-buckling instability, although at expense of the overall stiffness of the structure.

Cavallaro et al. (2014c) discussed the effects of the non-conservative loads of the follower type on the SBR. More important, the concept of bi-stability was discussed and shown to cause branch-jumping phenomena at load levels far below the nominal critical condition (identified through the nonlinear static analysis as the snap-buckling). This has theoretically a tremendous impact on design of Joined Wings: under certain conditions an apparently safe and quasi-linear steady-state condition may actually be unsafe if the post-critical analysis is ignored. Further investigations showed also stable branches completely detached from the main branch, suggesting that path-following techniques (like the arc-length) are not sufficient to unveil the whole picture.

This work will extend the last efforts introducing aerodynamic forces and investigating the nonlinear response of the Joined Wings, with particular focus on the stability property of the system (concept of snap-divergence) and on the differences with the cases in which mechanical loads (see Demasi et al., 2013b; Cavallaro et al., 2012, 2014c) are applied. For the first time on Joined Wings, post-divergence branches will be obtained and critically analyzed.

2. Contribution of the present study

It is common practice in the industry (e.g., ZONA Technology Inc., 2004; Rodden and Johnson, 1994) to calculate the divergence directly with the solution of an eigenvalue problem or via flutter analysis. The freestream velocity corresponding to the divergence is in general different than the one corresponding to the aeroelastic dynamic instability (flutter), thus, it has to be assessed which one represents the critical operative situation.

The above approaches, however, are based on an assumption that the structural properties of the system remain approximately constant. An open question is then how the divergence speed is calculated for a wing systems which experiences important geometric nonlinearity and how the divergence is precisely defined. This aspect is extensively addressed in the present work. It will also be assessed whether the eigenvalue approach, used to calculate the divergence speed, is reliable for Joined Wings.

A further contribution will be on the correlation of aeroelastic and structural static responses if mechanical conservative or nonconservative (follower type) loads are employed as a surrogate of the real aerodynamic forces. In fact, this approach is largely used as a mean of testing the structural response before more sophisticated and expensive campaigns are carried out. How reliable is this approach for Joined Wings? And, if not, could it at least give a conservative estimate?

Starting from the above points, the *real divergence* occurrence is more critically analyzed, and physical insight is gained by means of comparisons with previous results presented in the literature. In particular, aeroelastic load redistribution, overconstrained nature of Joined Wings and bending/stiffness coupling are discussed.

This work will also introduce the theoretical foundation of branch-follower numerical technique for static aeroelastic problems. These techniques are necessary to completely track the aeroelastic response, also after a critical (or turning) point is encountered.

2.1. On the importance of a conceptual study of Joined Wings

One conceptual question is how the findings of this work, carried out on simplified models, relate to a real flying aircraft. On this regard, several observations can be made:

1. Bi-stable regions (at macro-geometrical level) for a traditional configuration are generally not expected to be observed, whereas they are theoretically possible and shown for Joined Wing configurations. The presence of such regions impacts

the design, whereas, as argued in this work, not considering the likelihood of having this phenomenon may lead to catastrophic consequences. Even for stiffness distribution typical of real wings, it is not guaranteed that such instabilities are not present, since the Joined Wings share all the same inherent properties: overconstrained nature of the system associated with significant geometric nonlinearities.

2. A real aircraft should be designed to operate within the flight envelope and should be trimmed and stable on a flight mechanics point of view. In the here presented responses, the angle of attack is fixed and the aircraft is generally not trimmed. However, as previously discussed, one of the aims of this effort is to demonstrate snap-divergence and bi-stability occurrences for Joined Wings. They are driven by specific stiffness distribution, aerodynamic load, its repartition among the wings (which encompasses aspects as trim, angle of attack etc) and overconstrained nature of the system. Thus, it is theoretically possible to observe these catastrophic phenomena also on realistic configurations operating within the flight envelope.
3. The design of a real aircraft is a significant effort, and should never be carried out on innovative joined-wing configurations without exploring the whole scenario. Conceptual works, as the present one, are in the authors' opinion a necessity and good practice when tackling a tremendous effort like aircraft design. In fact, understanding why complex and counterintuitive phenomena eventually occur in Joined Wings is practically impossible (and expensive) when the number of design parameters/degrees of freedom is relatively large.
4. Bending/torsion coupling/aeroelastic tailoring is important in aeroelastic design. Its impact is further enhanced considering also the effects of the overconstrained nature of the system and the possibility of having multiple load paths. Since all Joined Wings feature the above properties, insight gained for one specific model (as those here presented) may have a valuable impact on the design of another one (for example, a realistic one).

3. Present nonlinear aeroelastic capability

To investigate the role of geometric structural nonlinearities in presence of attached flow, an appropriate in-house aeroelastic framework has been selected. On the structural side, a corotational finite element based on the linear membrane constant strain triangle (CST) and the flat triangular plate element (DKT) is employed. The *structural tangent matrix* $\boldsymbol{K}_{ST}$ is sum of two contributions: the elastic stiffness matrix, $\boldsymbol{K}_E$, and the geometrical stiffness matrix, $\boldsymbol{K}_G$. The formulation is based on works presented in Levy and Spillers (2003) with several corrections and improvements (e.g., Rankin and Nour-Omid, 1988) to the original effort.

The aerodynamic loads are evaluated through a steady incompressible VLM (see Katz and Plotkin, 2001) (Vortex Lattice Method) approach. The wing is subdivided into wing surfaces, each meshed as shown in Fig. 1. Each mesh element, called panel, is associated to a horseshoe vortex, a load point (where the aerodynamic force is applied) and a control point (where the Wall Tangency Condition – WTC – is imposed). The main assumption of the VLM is attached flow. Being geometrically nonlinear structural effects relevant for Joined Wings even for linear aerodynamics and attached flow, the current aerodynamic model is capable of capturing the main qualitative aspects of this work.

The deformation of the structure is taken into account when WTC is calculated. Splining is used to determine the slopes at the control points of the aerodynamic panels from the knowledge of the structural deflections on the structural nodes

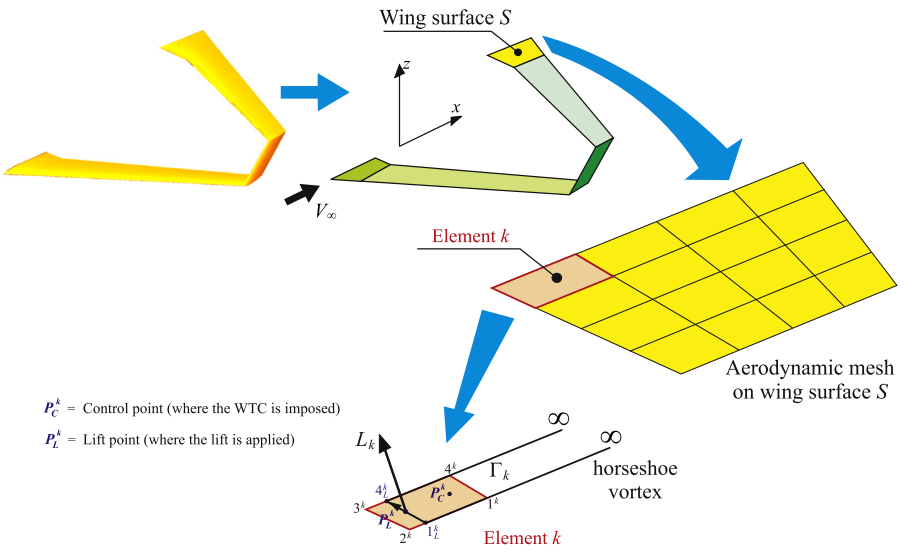

Fig. 1. Incompressible vortex lattice method: wing system, aerodynamic mesh and panel.

(not depicted in Fig. 1 for simplicity). A more detailed discussion of the interface technique (load/displacement transferring between the aerodynamic and structural meshes) as well as aerodynamic solver is shown in Cavallaro et al. (2014b).

The nonlinear aeroelastic equations are solved by adopting iterative techniques discussed in Section 3.1. After each iteration a displacement vector is obtained, rigid body motion is eliminated and the pure elastic rotations and strains are found. Using these quantities the internal forces are updated for the next iteration. Adding the aerodynamic effects provides unique features that need to be specifically addressed. This is discussed in detail in the following sections.

3.1. Solution of the nonlinear aeroelastic equations via arc length technique

The wings are subjected to aerodynamic loads, indicated with $\boldsymbol{L}$. A reference freestream velocity, V_∞^{ref}, and air density ρ_∞ are chosen, and corresponding dynamic pressure $p_{\text{dyn}}^{\text{ref}} = \frac{1}{2}\rho_\infty (V_\infty^{\text{ref}})^2$ is evaluated. Two iterative procedures are employed in the static analysis: Newton–Raphson and arc length methods. Some theoretical aspects are now outlined with emphasis on the aeroelastic nature of the system under investigation.

The term *iteration* used in the following refers to the repetitive refinement of a nonlinear solution for an incremental load step μ. In nonlinear static analysis the load vector needs to be "gradually" applied to the structure for both facilitating convergence and drawing the whole curve response. This is practically achieved with the introduction of a load level Λ which represents the fraction of dynamic pressure (compared to the reference assigned value) applied to the system. Within a given load step μ several iterations take place before the numerical method converges with a prescribed tolerance.

There is a conceptual difference between the terms load step and iteration: at the beginning of a load step the equilibrium equations are "exactly" satisfied (within numerical tolerance), whereas at each iteration within a load step the static equilibrium is in general not satisfied and there is an error that needs to be reduced with additional subsequent iterations before a new load step is started. The analysis terminates when the entire reference dynamic pressure is applied.

To present the theoretical derivation, the concept of cumulative displacement vector $\boldsymbol{U}$ needs to be defined. $\boldsymbol{U}$ is a vector whose entries are the summation of all the displacements that occurred at all the previous numerical evaluations. If the undeformed structure is provided with an angle of attack (constant or variable twist) then there are aerodynamic forces even at the very first iteration of the numerical procedure. This is taken into account by defining $\boldsymbol{U}$ to be exactly a null vector only if there is no angle of attack (and so no aerodynamic forces are present). If a given incidence is provided, an appropriate initial value of $\boldsymbol{U}$ must be given so that the aerodynamic forces are correctly computed, accordingly with Eq. (1)).

At the *beginning* of the nth iteration of a certain load step μ the aerodynamic loads are indicated with $\boldsymbol{L}_{\text{str}}^{\text{step }\mu\text{ iter }n}$. According to the present formulation, it can be demonstrated (see Demasi and Livne, 2009c), that these forces have the following expression:

$$\boldsymbol{L}_{\text{str}}^{\text{step }\mu\text{ iter }n} = p_{\text{dyn}}^{\text{step }\mu\text{ iter }n}\boldsymbol{C}\cdot\boldsymbol{U}^{\text{step }\mu\text{ iter }n}, \tag{1}$$

where $\boldsymbol{C}$ is an aerodynamic constant matrix (this matrix would be load step dependent if the compressibility correction is added). $\boldsymbol{U}^{\text{step }\mu\text{ iter }n}$ is the cumulative displacement array at the beginning of the n th iteration. Similarly, $p_{\text{dyn}}^{\text{step }\mu\text{ iter }n}$ represents the dynamic pressure *gradually* applied to the system evaluated before iteration n is performed. Recalling the definition of the load level Λ, it is possible to write

$$p_{\text{dyn}}^{\text{step }\mu\text{ iter }n} = \Lambda^{\text{step }\mu\text{ iter }n}\cdot p_{\text{dyn}}^{\text{ref}}. \tag{2}$$

When the arc length method is adopted, the unknowns are represented by the incremental displacement vector $\boldsymbol{u}^{\text{step }\mu\text{ iter }n}$ (which is referred to the coordinates at the beginning of the current iteration, following the concept of *Updated Lagrangian Formulation*) and the load level increment $\lambda^{\text{step }\mu\text{ iter }n}$. It holds

$$\boldsymbol{U}^{\text{step }\mu\text{ iter }(n+1)} = \boldsymbol{U}^{\text{step }\mu\text{ iter }n} + \boldsymbol{u}^{\text{step }\mu\text{ iter }n}, \tag{3}$$

and

$$\Lambda^{\text{step }\mu\text{ iter }(n+1)} = \Lambda^{\text{step }\mu\text{ iter }n} + \lambda^{\text{step }\mu\text{ iter }n}. \tag{4}$$

The definition of the aeroelastic tangent matrix, in the framework of arc length method, could be derived using the concept of *residual*. This is now presented in detail starting from the theory of generic follower forces recalled in Cavallaro et al. (2014c).

Both the external aerodynamic loads $\boldsymbol{L}$ and the internal forces $\boldsymbol{F}_{\text{int}}$, due to the deformation of the structure, are a function of the cumulative displacement $\boldsymbol{U}$. Moreover, the aerodynamic loads are also a function of the load level Λ. The residual $\mathcal{R}$ is defined as the difference between the aerodynamic loads and the internal forces. If convergence has been reached, then the equilibrium is satisfied and the residual is (almost) zero.

In mathematical terms the residual (or unbalanced load) is the following:

$$\mathcal{R}(\boldsymbol{U},\Lambda) = \boldsymbol{L}(\boldsymbol{U},\Lambda) - \boldsymbol{F}_{\text{int}}(\boldsymbol{U}), \tag{5}$$

which, by means of equations shown in Demasi and Livne (2009c, 2009c), becomes

$$\mathcal{R}(\boldsymbol{U},\Lambda) = \Lambda\cdot p_{\text{dyn}}^{\text{ref}}\cdot\boldsymbol{C}\cdot\boldsymbol{U} - \boldsymbol{F}_{\text{int}}(\boldsymbol{U}). \tag{6}$$

Assume now that the starting state is identified by load step μ and iteration n and that the goal is to drive to zero the unbalanced load evaluated at the subsequent iteration. Then, a zero finding method, and in this case a Newton's method, could be applied leading to

$$\begin{aligned}\mathbf{0} = &\left[\frac{\partial \mathcal{R}(\mathbf{U},\Lambda)}{\partial \mathbf{U}}\right]^{\text{step } \mu \text{ iter } n} \left(\mathbf{U}^{\text{step } \mu \text{ iter } (n+1)} - \mathbf{U}^{\text{step } \mu \text{ iter } n}\right) \\ &+ \left[\frac{\partial \mathcal{R}(\mathbf{U},\Lambda)}{\partial \Lambda}\right]^{\text{step } \mu \text{ iter } n} \left(\Lambda^{\text{step } \mu \text{ iter } (n+1)} - \Lambda^{\text{step } \mu \text{ iter } n}\right) + \mathcal{R}^{\text{step } \mu \text{ iter } n},\end{aligned} \tag{7}$$

which is more conveniently rewritten as

$$\mathbf{0} = \left[\frac{\partial \mathcal{R}(\mathbf{U},\Lambda)}{\partial \mathbf{U}}\right]^{\text{step } \mu \text{ iter } n} \mathbf{u}^{\text{step } \mu \text{ iter } n} + \left[\frac{\partial \mathcal{R}(\mathbf{U},\Lambda)}{\partial \Lambda}\right]^{\text{step } \mu \text{ iter } n} \lambda^{\text{step } \mu \text{ iter } n} + \mathcal{R}^{\text{step } \mu \text{ iter } n}. \tag{8}$$

With $[\,]^{\text{step } \mu \text{ iter } n}$ it has to be intended that the derivatives are evaluated for $\mathbf{U}$ and Λ relative to load step μ and iteration n. The derivatives in Eq. (8) are calculated by using the expression for the residual (Eq. (6)):

$$\begin{aligned}&\left[\frac{\partial \mathcal{R}(\mathbf{U},\Lambda)}{\partial \mathbf{U}}\right]^{\text{step } \mu \text{ iter } n} = \Lambda^{\text{step } \mu \text{ iter } n} \cdot p_{\text{dyn}}^{\text{ref}} \cdot \mathbf{C} - \left[\frac{\partial \mathbf{F}_{\text{int}}(\mathbf{U})}{\partial \mathbf{U}}\right]^{\text{step } \mu \text{ iter } n}, \\ &\left[\frac{\partial \mathcal{R}(\mathbf{U},\Lambda)}{\partial \Lambda}\right]^{\text{step } \mu \text{ iter } n} = p_{\text{dyn}}^{\text{ref}} \cdot \mathbf{C} \cdot \mathbf{U}^{\text{step } \mu \text{ iter } n}.\end{aligned} \tag{9}$$

The definitions of aerodynamic tangent matrix $\mathbf{K}_A^{\text{step } \mu \text{ iter } n}$ and structural tangent matrix $\mathbf{K}_{ST}^{\text{step } \mu \text{ iter } n}$ are now introduced:

$$\begin{aligned}&-\Lambda^{\text{step } \mu \text{ iter } n} \cdot p_{\text{dyn}}^{\text{ref}} \cdot \mathbf{C} = \mathbf{K}_A^{\text{step } \mu \text{ iter } n} \\ &\left[\frac{\partial \mathbf{F}_{\text{int}}(\mathbf{U})}{\partial \mathbf{U}}\right]^{\text{step } \mu \text{ iter } n} = \mathbf{K}_{ST}^{\text{step } \mu \text{ iter } n}.\end{aligned} \tag{10}$$

Substitution of Eq. (10) into Eqs. (9) and (8) leads to

$$\begin{aligned}\mathbf{0} = &-\underbrace{\left[\mathbf{K}_A^{\text{step } \mu \text{ iter } n} + \mathbf{K}_{ST}^{\text{step } \mu \text{ iter } n}\right]}_{\mathbf{K}_T^{\text{step } \mu \text{ iter } n}} \mathbf{u}^{\text{step } \mu \text{ iter } n} \\ &+ \lambda^{\text{step } \mu \text{ iter } n} \cdot p_{\text{dyn}}^{\text{ref}} \mathbf{C} \cdot \mathbf{U}^{\text{step } \mu \text{ iter } n} + \mathcal{R}^{\text{step } \mu \text{ iter } n},\end{aligned} \tag{11}$$

where $\mathbf{K}_T^{\text{step } \mu \text{ iter } n}$ is the aeroelastic tangent matrix obtained by adding the aerodynamic and structural contributions. As apparent from Eq. (11) both $\mathbf{u}^{\text{step } \mu \text{ iter } n}$ and the applied load fraction $\lambda^{\text{step } \mu \text{ iter } n}$ are unknowns in the arc length method. Different closing constraint equations could be employed, leading to different arc length methods, such as *Crisfield*, *Riks-Wempner* or *Ramm*'s (also called modified Riks) methods, (e.g., Riks, 1979; Crisfield, 1991). As an example, application of Crisfield's cylindrical arc length method (see Crisfield, 1991) leads to the following constraint:

$$\left|\mathbf{u}^{\text{step } \mu \text{ iter } n} + \mathbf{U}^{\text{step } \mu \text{ iter } n} - \mathbf{U}^{\text{step } \mu \text{ iter } 1}\right|^2 = \Delta l^2, \tag{12}$$

where Δl has been previously fixed. Eqs. (11) and (12) give raise to a second order relation for the quantity $\lambda^{\text{step } \mu \text{ iter } n}$.

It is worth to notice that the success of one of the arc length strategies in overcoming limit points is problem dependent. In some cases some strategies perform better than others, thus it may be necessary to switch between them to track the whole response curve.

3.2. Validation of the nonlinear aeroelastic code

The present capability has been validated comparing results with commercial software Nastran (see Demasi and Livne, 2009b). The arch length techniques have also been validated for the cases of mechanical loads in recent works (i.e., Demasi et al., 2013b; Cavallaro et al., 2012, 2014c).

4. Snap-divergence and its mathematical definition

To introduce the concept of snap-divergence, consider the *pure structural case* in which only mechanical forces act. In that case it is possible to define a *buckling load* obtained via eigenvalue analysis. This investigation of the stability properties could be improved by linearizing about a steady state equilibrium obtained with a fully nonlinear static analysis. However, it is also possible to define (if exists for the case under investigation) the *snap-buckling load* as the one corresponding to the true critical point, in which the structural tangent stiffness matrix becomes singular.

These definitions involve a precise mathematical event (singularity of a matrix). However, nonlinear analyses may also show responses with a progressive softening (see for example Demasi et al., 2013b; Cavallaro et al., 2012), in which very small load increments lead to large displacements: this is, de facto, a “practical” instability. It may be then too restrictive and

unsafe to base the buckling concept on the above definition (singularity of the matrix) only. It is also true that a more general definition of instability may not be easily identified, depending on the particular problem.

If the steady aeroelastic problem is now considered, the system's tangent matrix has also the contribution of the aerodynamics. The same considerations about the stability and singularity of the matrix apply. To distinguish this same event between the structural and aeroelastic cases, the aeroelastic instability is termed “snap-divergence” (true divergence). The word “snap” is here adopted on purpose, since historically the aeroelastic divergence was typically performed with the eigenvalue analysis, and also because of the tendency to “snap” of the configuration on verge of instability.

It may be argued that the *post-divergence* regime is completely meaningless when an aeroelastic case is investigated: after the snap-divergence instability is reached the system would naturally experience a snap and *try* to reach a state on the stable post-critical branch. However, as previously discussed, the knowledge of the static post-critical regime may give indication on bistability and associated risks as the so-called “branch-jumping” instability, see for example results presented in Cavallaro et al. (2014c).

Actually, this sudden change is inherently a dynamic phenomenon and thus, inertial forces and time-dependent aerodynamic effects must be taken into consideration to properly model the response of the structure (see Dowell et al., 2003). Limit Cycle Oscillations can develop as discussed in Cavallaro et al. (2014b).

5. Linearized divergence speed via eigenvalue approach

The classic approach to evaluate divergence speed is to solve an eigenvalue problem. The starting configuration about which a linearization is carried out can be the fundamental (undeformed) one or a deformed steady state equilibrium corresponding to the dynamic pressure $p_{\text{dyn}}^{\text{ss}}$.

The structural tangent matrix corresponding to the associated steady state (i.e., after the numerical simulations are completed and the nonlinear response has been determined up to the dynamic pressure $p_{\text{dyn}}^{\text{ss}}$) is indicated with the symbol $\boldsymbol{K}_{ST}^{\text{ss}}$. Observing that the aerodynamic tangent matrix depends on the dynamic pressure, it is deduced that the matrix corresponding to the (unknown) linearized divergence condition is

$$\boldsymbol{K}_A^D = -p_{\text{dyn}\ D}^{\text{lin}}\boldsymbol{C}. \tag{13}$$

The dynamic pressure is treated as an unknown and needs to be found. Let $p_{\text{dyn}\ D}^{\text{lin}}$ be the *candidate* dynamic pressure corresponding to the instability condition (according to the linearized eigenvalue divergence analysis). The linearized divergence speed is the non-trivial solution (i.e., $\boldsymbol{u} \neq \boldsymbol{0}$) of the following aeroelastic equation:

$$\left(\boldsymbol{K}_{ST}^{\text{ss}} + \boldsymbol{K}_A^D\right)\boldsymbol{u} = \boldsymbol{0}. \tag{14}$$

A non-trivial solution is found when the aeroelastic matrix, obtained by adding the structural and aerodynamic contributions, is singular. This condition is now exploited by substituting Eq. (13) into Eq. (14):

$$(\boldsymbol{K}_{ST}^{\text{ss}} - p_{\text{dyn}\ D}^{\text{lin}}\boldsymbol{C})\boldsymbol{u} = \boldsymbol{0}. \tag{15}$$

This is an eigenvalue problem. The eigenvalues represent the dynamic pressure corresponding to the linearized divergence.

Only *positive* eigenvalues have physical meaning and, among them, the smallest is the relevant one.

6. Description of the analyzed Joined Wing configurations

Two configurations will be analyzed in this paper. The first one, depicted in Fig. 2, is a Joined Wing (see Demasi and Livne, 2009b) (named *JW70*) in which the joint is not located at the tip of both wings.

The second layout (Fig. 3) is a PrandtlPlane-like configuration (see Demasi et al., 2013b; Cavallaro et al., 2012, 2014a) featuring a swept-back lower wing and a swept-forward upper wing. It is named *PrP40*.

For the aerodynamic analysis, the surfaces have been discretized employing 8–12 elements in the chordwise direction. The total number of aerodynamic panels is then approximately between 600 and 3000 for the different cases. Convergence of the aerodynamic loads has been verified already for the coarse discretization.

The adopted material is a typical aluminium, featuring Young's modulus $E_{\text{REF}} = 6.9 \times 10^7 (\text{Kg/mm s}^2)$ and a Poisson's ratio $\nu_{\text{REF}} = 0.33$. Both models' dimensions are selected to be consistent with the ones corresponding to wind-tunnel scaled models.

The density of the air is chosen to be the standard air density ($\rho_\infty = 1.225\ \text{kg/m}^3$), whereas the geometric angle of attack is set to 1°. In order to get different static conditions, the onset free-stream velocity is varied (through the parameter Λ). The aerodynamic forces change during the iterative process because the deformation induces a change of local angles of attack and the freestream velocity is also changed (through Λ). This is taken into account by the aerodynamic tangent matrix $\boldsymbol{K}_A$ previously discussed. The aerodynamic forces are then follower forces in the sense that their magnitude depends on the structural deformation. Actual aerodynamics forces are also follower in the direction, and more refined models are widely used in the literature (see Cavallaro et al., 2014c, 2014b). For a study of mechanical forces that change direction during the deformation of the Joined Wing, refer to Cavallaro et al. (2014c).

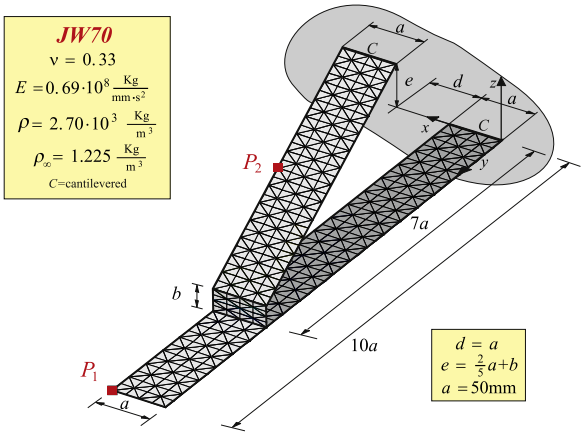

Fig. 2. *JW70* model. The joint is located at 70% of the wing span. The thickness of the different parts of the structure is equal to 0.7 mm. The joint's height is $b=20$ mm.

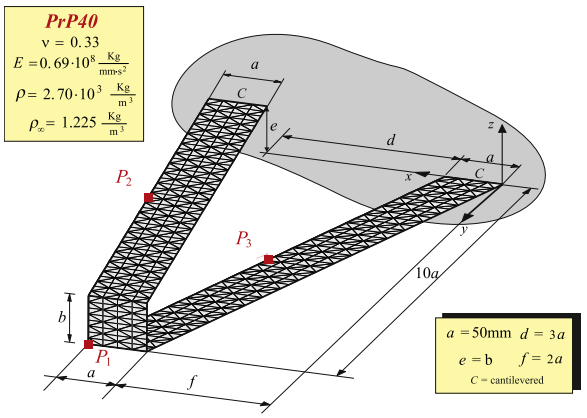

Fig. 3. PrandtlPlane Joined Wing model *PrP40*. The joint is located at the tip of the wings. The thickness of the different parts of the structure is equal to 1.0 mm. The joint's height is $b=40$ mm.

Convergence study on the configurations has been carried out, showing that the meshes represented in Figs. 2 and 3 give results within 1% of the converged response.

7. Nonlinear divergence analysis of configuration *JW70*

In this section the baseline configuration *JW70* is analyzed from a static nonlinear aeroelastic perspective. The stability properties are also investigated with linear capabilities (linear and linearized divergence analyses) in order to assess the reliability of classical aeroelastic computational methods. In addition to the aeroelastic simulations, pure structural investigations are also carried out. The structural response of the system subjected to both conservative and follower mechanical loads is compared with the aeroelastic analysis with the aim of providing indications on the appropriateness of using mechanical loads to mimic real aerodynamic forces (see also Bond et al., 2012).

The static aeroelastic response is obtained by gradually increasing the aerodynamic speed V_∞. The typical displacement-velocity curves (see Figs. 4 and 5) are then obtained for point P_1 located at the tip of the lower wing and for point P_2 positioned at the mid-span of the upper wing (see Fig. 2 to graphically localize these points).

It is clear that a snap-divergence phenomenon occurs: with reference to Figs. 4 and 5, an infinitesimal increment of speed at state B would determine an impossibility to find a continuously adjacent static equilibrium configuration. On the contrary, the new equilibrium point would be C, characterized by the same flow speed of state B which is the *snap-divergence speed* V_∞^{CR}, equal to 34.1 m/s. Notice that, at state B the *system tangent matrix* is exactly singular, thus, the instability has a well defined mathematical characterization.

As already discussed in Cavallaro et al. (2014c), snap instabilities are inherently dynamic phenomena. In the case of conservative mechanical forces, a snap from state B would physically lead to state C (after a transient has been extinguished through structural damping, and if the forces remain constant throughout the process). However, when aerodynamic forces

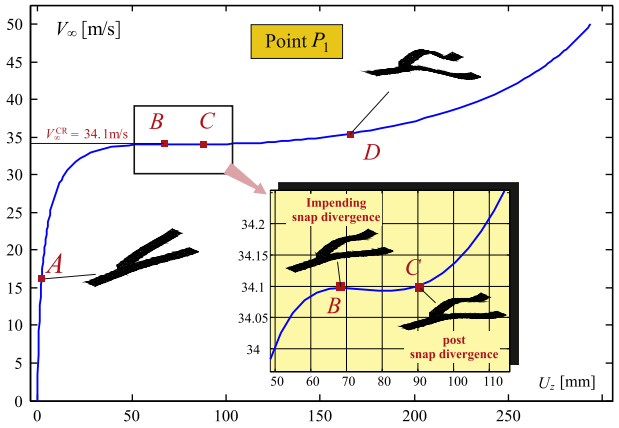

Fig. 4. Configuration *JW*70: flow speed V_∞ (in m/s) versus cumulative vertical displacement U_z (in mm) for lower wing's tip point P_1. The flow is directed along the *x*-axis, and the geometry is rotated to 1° in order to create an initial angle of attack. A zoom of the critical point area is provided.

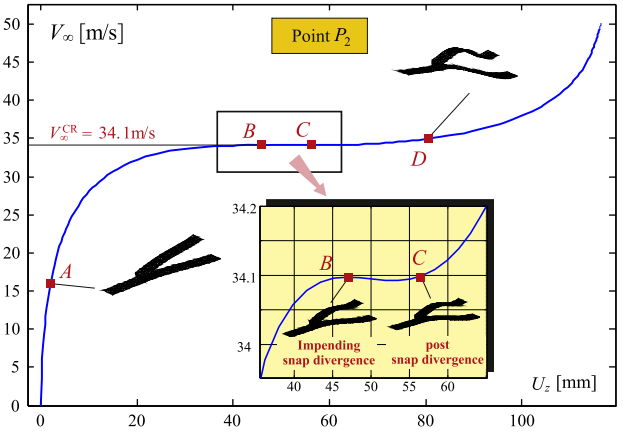

Fig. 5. Configuration *JW*70: flow speed V_∞ (in m/s) versus cumulative vertical displacement U_z (in mm) for upper wing's midspan point P_2. The flow is directed along the *x*-axis, and the geometry is rotated to 1° in order to create an initial angle of attack.

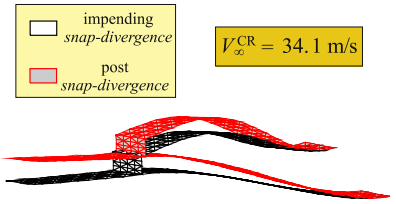

Fig. 6. Configurations at states immediately preceding and following the snap-divergence (states B and C in Fig. 5).

are considered, this may not be the case. The dynamical system in fact may diverge to other-than-fixed-point kind of *attractors*. An example could be the phenomenon of limit cycle oscillation (LCO), in which an infinitesimal small perturbation from a steady state (fixed point) may lead to a closed periodic pattern (see for example Cavallaro et al., 2014b). To check this option a linearized flutter analysis is performed with the tool described in Demasi and Livne (2009a,c), and it is ascertained that flutter speed is higher than snap-divergence one's.

The configurations at impending snap-divergence (state *B*) and the one immediately after it (state *C*) are reproduced in Fig. 6. Moreover, Fig. 7 shows the span-wise distribution of lifting forces and twist distribution, for different flow speeds (corresponding to the points *A* through *D* in Figs. 4 and 5).

The sectional lifting forces of Fig. 7 are evaluated as the sum of the aerodynamic loads projected on the structural nodes lying on the same cross-section. The geometrical twist of each cross section is calculated considering the up- and down-stream nodes on the same station at fixed spanwise coordinate, and simply evaluating the geometrical angle between the line joining these two points and the *x*-axis (the deformation in the section plane may be considered of second order).

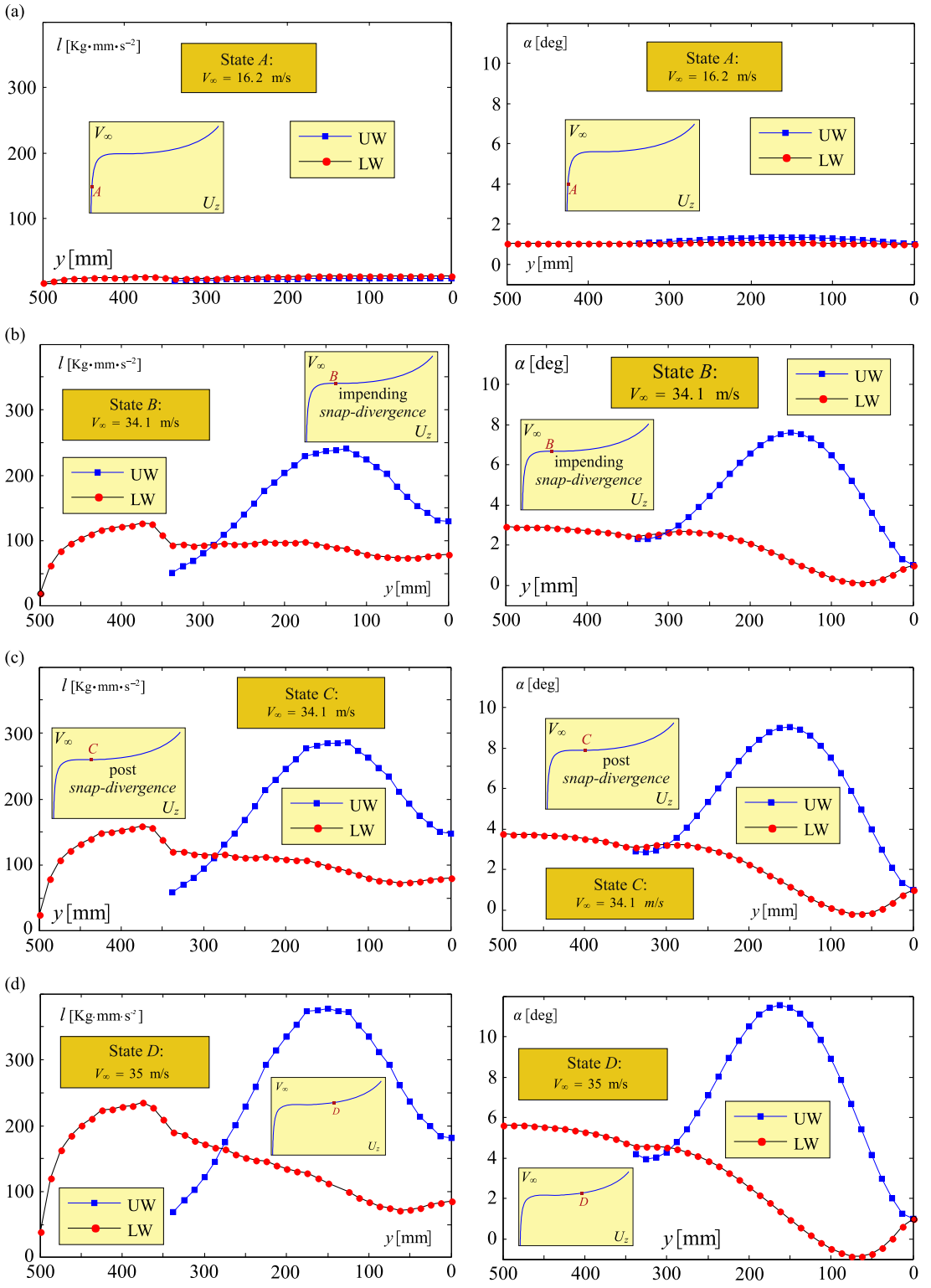

Fig. 7. On the left column: sectional lift distribution on the wings. On the right column: geometrical twist of the sections. Results are shown for different flow speeds, as indicated in the figure. All the plots refer to both the upper (UW) and lower wings (LW). (a) Case with $V_\infty = 16.2$ m/s (state *A* in Fig. 4). (b) Case with $V_\infty = 34.1$ m/s, impeding snap-divergence (state *B* in Fig. 4). (c) Case with $V_\infty = 34.1$ m/s, post snap-divergence (state *C* in Fig. 4). (d) Case with $V_\infty = 35$ m/s (state *D* in Fig. 4).

7.1. Physical interpretation of the aeroelastic response

Fig. 7 could be used to attempt a physical interpretation of the aeroelastic response as follows. Initially both the wings are producing lift, however, due to the joint connection, the upper wing experiences an increase of angle of attack (positive torsion), whereas for the inner part of the lower wing, the change in torsion is relatively smaller (see Fig. 7(a)). This coupling comes from the geometry: the upper wing has a negative sweep angle and, thus, a vertical displacement of the tip produces both a bending and a positive torsion. However, the upper wing increment of angle of attack is partially counteracted by the lower wing which shows a smaller increment in twist. This coupling is more pronounced when deformation takes place. Notice that, even for not highly deformable Joined Wings, the coupling and consequent load redistribution has a profound impact on the design since the trim conditions are affected.

When the snap-divergence velocity is reached the structural stiffness of the system cannot efficiently resist the aerodynamic actions. There is a general large increment of the section twist, especially localized in the upper wing, as it can be verified in Fig. 7(b)–(d).

7.2. Comparison between eigenvalue and nonlinear divergence analysis

This study assesses how reliable the eigenvalue approach (as described in Section 5) is when geometric structural nonlinearities need to be taken into account in the calculation of the divergence conditions (V_∞^{ss}). Different starting steady states are considered when linearized eigenvalue analyses are carried out. That is, the divergence speed is calculated using the classical eigenvalue approach but the structural stiffness matrix used for the numerical evaluations is the one corresponding to a configuration relative to a flow speed between 0 and 33.5 m/s (Fig. 4 can be used to locate the steady states configurations in the speed-displacement response curve).

Results in terms of predicted divergence speed are depicted in Fig. 8. The linearized divergence speeds $V_{\infty D}^{lin}$ are plotted against the freestream velocities (V_∞^{ss}) associated with the configurations chosen for linearization. As deduced from Fig. 8, the linearization performed about the undeformed configuration provides a divergence speed $V_{\infty D}^{lin}$ which is about 50% larger than the true static instability condition identified by the snap-divergence speed V_∞^{CR}. More than the extent of the discrepancy, it is important to observe that the error is not conservative because the speed at which the instability occurs is overestimated.

To have more reliable results one might think to track the nonlinear response until a “reasonable” value of the speed is reached, and then linearize about that steady state configuration when doing the eigenvalue analysis. However, a higher freestream velocity about which the linearization is performed implies a higher computational cost, since a larger portion of the nonlinear response needs to be tracked. Unfortunately, from Fig. 8 it is clear that there are practically no accuracy improvements for the linearized divergence speed prediction, until very close to the snap-divergence speed. Notice how, graphically, there is a region, bounded by the condition $V_{\infty D}^{lin} = V_\infty^{ss}$, for which the configurations is not stable.

Summarizing, the eigenvalue approach for predicting the divergence speed appears to be *unreliable* (large errors compared to the true static instability velocity) and *unsafe* (it overestimates the critical speed). It could be reliable only if all the response curve to almost the snap-divergence speed is tracked, which is meaningless since the cost would be of the same order as for a complete nonlinear analysis.

As a consequence, linear divergence analysis is not amenable to be used as a preliminary design tool (multidisciplinary design optimization) for Joined Wings.

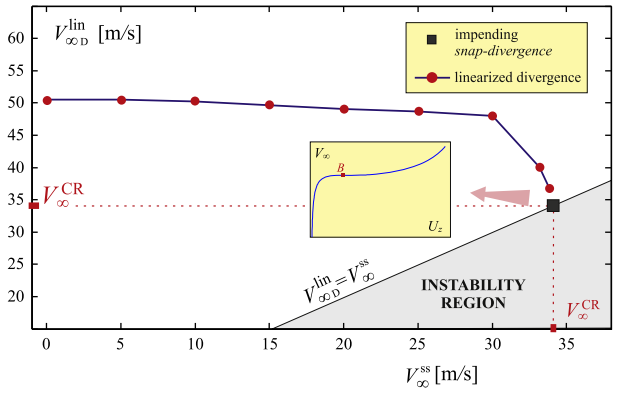

Fig. 8. Outcome of linearized divergence analysis: on the abscissa the speeds associated with the deformed configuration chosen for linearization are depicted (i.e., V_∞^{ss}), whereas, on the ordinate, the divergence speeds obtained via eigenvalue approach are shown (i.e., $V_{\infty D}^{lin}$). The shaded region is bounded by $V_\infty^{ss} = V_{\infty D}^{lin}$, which is the condition for snap-divergence to occur.

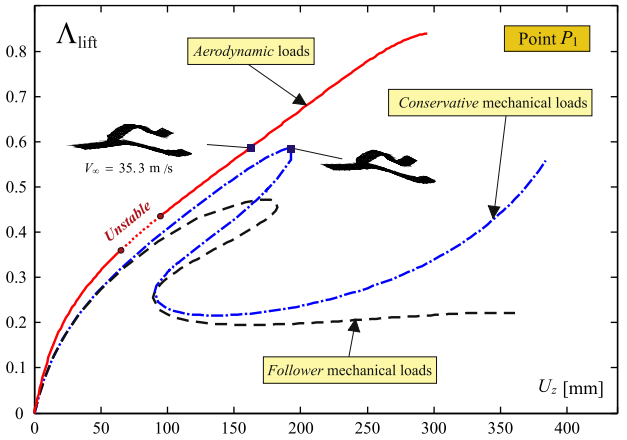

Fig. 9. JW70 configuration: normalized load level Λ_{lift} versus cumulative vertical displacement U_z for lower wing's tip point P_1 when conservative and follower mechanical forces and aerodynamic loads are considered.

7.3. Mechanical and aerodynamic forces: a comparison

The use of structural loads may be an interesting option to readily have a first guess estimate of the deformation given by the aerodynamic loads, or also to experimentally apply the forces to the structure. In this regard, past computational and experimental work on Joined Wings studied the nonlinear response due to mechanical loads (see Kim et al., 2011; Bond et al., 2012). It is then important to investigate such an approach, and in particular, assess whether it is conservative.

Two mechanical types of loadings are then considered. The first class is represented by a load-per-unit-of-surface (pressure) always vertically directed (*conservative* mechanical loads). The second type is a pressure load which remains perpendicular to the structure during the deformation process (*follower* mechanical loads). In both types of load the nominal value of the pressure is $p = 0.55125$ Kg/(mm s^2), corresponding to the dynamic pressure of air (at sea level) with a speed of 30 m/s. Refer to Demasi et al. (2013a, Figs. 9–12) for the detailed responses.

To correlate the predictions of the mechanical and aerodynamic loads cases the *global vertical load* (lift) is chosen as a comparison parameter. Moreover, the resultant of a force per unit area of 0.55125 Kg/(mm s^2) directed along the z-axis is chosen as the nominal vertical load. The amount of lift produced/acting on the system at a given state is finally written in dimensionless form by dividing it by the lift calculated as described above. The dimensionless parameter Λ_{lift} is then defined, and plays a similar role as the one played by Λ earlier adopted. Notice that $\Lambda_{\text{lift}} = \Lambda$ for the conservative mechanical forces because they are always directed along z.

Fig. 9 compares the responses when mechanical and aerodynamic loads are applied to the structure. The same trend is observed for a significant portion of graph. In other words, mechanical conservative loads may be used to assess the stiffness of the structure at least up to a certain level (here with stiffness it is qualitatively intended the ratio of the generated lift to the displacement/deformation of the structure).

At first glance, the aerodynamic case may even look more favorable, since an appropriate lift may be achieved without incurring in loss of stiffness (as it happens for both the conservative and follower mechanical load cases as consequence of the snap-phenomenon). However, this graph hides an important difference between the aerodynamic and mechanical loads: the aerodynamic forces are associated to a flow speed. Although the response for the aerodynamic case looks smooth and far from any instability, actually, in practice, the region $\Lambda_{\text{lift}} = [0.3,\ 0.5]$ corresponds to an *unstable* condition (see for example Fig. 4 where the snap-divergence is depicted). As it could be inferred inspecting Fig. 10, a small perturbation/variation of the flow speed produces relatively large increments of the angle of attack of the structure with associated large increments in the lift. This emphasizes that even if mechanical forces may sometimes give good indication of load–displacement response, they cannot provide inherent information on the real stability properties of the system.

Loading the Joined Wing with follower mechanical forces represents a really penalizing test. When loaded, the structures undergoes large displacements with the effect that the surface normals have a diminishing vertical component. Acting the (follower) pressures perpendicularly to the surface, the lift begins to decrease after a critical deformation.

For a more accurate analysis, a more advanced aerodynamic model should be adopted (see Cavallaro et al., 2014b). In fact, with the present capability, the aerodynamic forces are oriented perpendicularly to the initial configuration, changing their magnitude (but not their direction) with progressive deformation of the structure (see Demasi and Livne, 2009c). The severity of a follower structural load approach is then expected when compared with the present aerodynamic capability.

8. Nonlinear divergence analysis of configuration *PrP40*

The configuration *PrP40*, whose geometrical and material details are described in Section 6 and depicted in Fig. 3, is here considered.

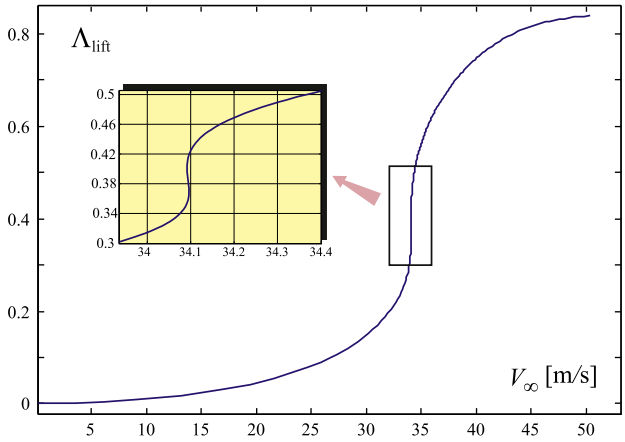

Fig. 10. *JW70* configuration: normalized load level Λ_{lift} versus flow speed.

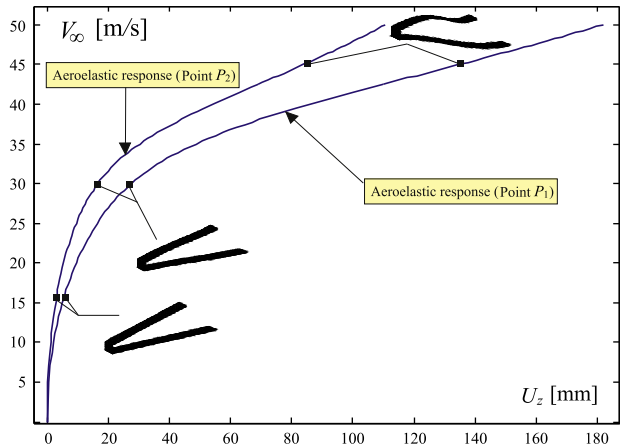

Fig. 11. Flow speed V_∞ (in m/s) versus cumulative vertical displacement U_z (in mm) for lower wing tip point P_1 and upper wing midspan point P_2 of the joined-wing layout *PrP40*. The flow is directed along the *x*-axis, and the geometry is rotated to 1° in order to create an initial angle of attack.

As for the *JW70* configuration, stability properties will be assessed with the aid of linearized divergence eigenvalue analysis. Moreover, the nonlinear aeroelastic response will be compared to results presented in Demasi et al. (2013b) and Cavallaro et al. (2014c), where the same *PrP40* configuration undergoes mechanical structural conservative and follower loads respectively. As a final task a discussion about divergence, bending/torsion coupling, and overconstrained nature of Joined Wings will be given. To support the discussion, a further analysis will be introduced, i.e., the response of *PrP40* with unswept wings.

The aeroelastic response for points P_1 and P_2, on the lower wing tip and upper wing mid-span respectively (as depicted in Fig. 3), is shown in Fig. 11. It is interesting to observe that *no* snap-instability phenomenon is present. From a practical perspective, however, there is a consistent loss in stiffness after the speed of 30 m/s.

8.1. Divergence analysis via eigenvalue approach

Different steady states about which the linearization is carried out are considered. The results are reported in Fig. 12. If the softening tendency seen starting from speed of 15 m/s (refer to Fig. 11) is not considered as critical from a practical perspective, then the linearized divergence analysis correctly suggests that no stability issue would arise in the range of considered speeds. If the linearization is carried out for larger freestream velocities, then it is possible to observe a trend of decreasing predicted divergence speeds (see Fig. 12). This behavior suggests that a softening is in place.

8.2. Mechanical and aerodynamic forces: a comparison

References Demasi et al. (2013b) and Cavallaro et al. (2014c) discussed the structural nonlinear analysis of the configuration *PrP40* subjected to mechanical loads and focused on the snap phenomenon. However, such an instability

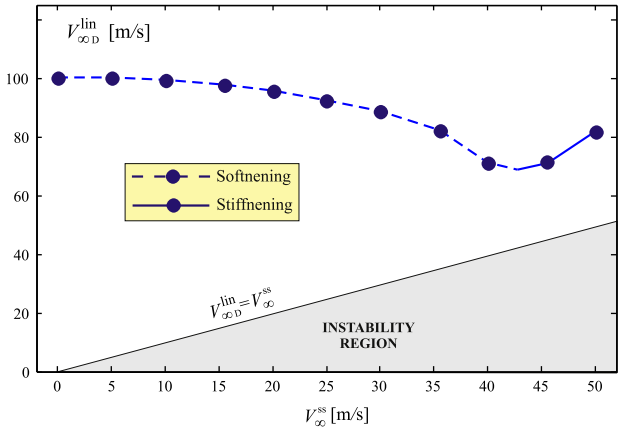

Fig. 12. Outcome of linearized divergence analysis: on the abscissa the speeds associated with the deformed configuration chosen for linearization are depicted (i.e., V^{ss}_{∞}), whereas, on the ordinate, the divergence speeds obtained via eigenvalue approach are shown (i.e., $V^{lin}_{\infty D}$). The shaded region is bounded by $V^{ss}_{\infty} = V^{lin}_{\infty D}$, which is the condition for snap-divergence to occur.

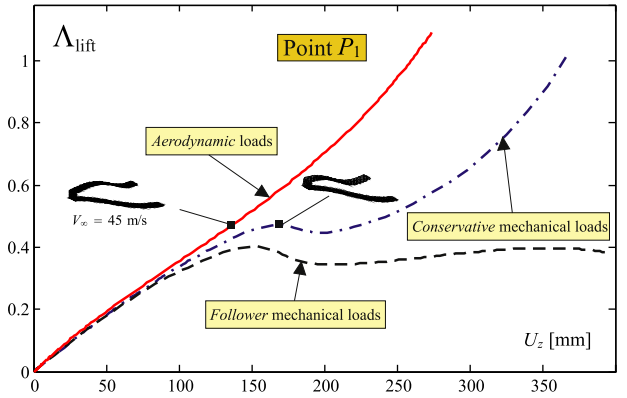

Fig. 13. Normalized load level Λ_{lift} versus cumulative vertical displacement U_z for lower wing's tip point P_1 of the joined-wing layout *PrP40* when conservative, follower and aerodynamic loads are applied.

was not detected in the present work when aerodynamic forces were applied. In an effort of further investigating the differences produced by the application of loads of different nature (mechanical and aerodynamic forces), it is convenient, for a quantitative comparison, to define a nominal force which will be used for normalization purposes. Following the same logics adopted for the *JW70* case, a vertical force per unit of area $p = 0.55125$ Kg/(mm s^2), corresponding to the dynamic pressure of air (at sea level) with a speed of 30 m/s, is applied and its resultant is adopted as a reference force to define a dimensionless parameter Λ_{lift}. That is, Λ_{lift} is introduced as the ratio of the global vertical (along z-axis) force due to mechanical/aerodynamic forces to the above defined reference vertical force. For the case of conservative loads presented in Demasi et al. (2013b), the forces are always vertical, thus, there is equivalence between Λ and Λ_{lift}.

The normalized curves are plotted in Fig. 13 for the point P_1 (the tip of the lower wing) in terms of vertical displacement against the vertical load level Λ_{lift}. For the follower case (results presented in Cavallaro et al., 2014c) besides the snap-buckling, there is also a loss in capacity of producing vertical forces due to the progressive bending of the wing, (the normals to the finite elements assume slowly a predominant horizontal direction). On the other hand, the aerodynamic case shows an increasing ability to produce lift with the deformation.

8.2.1. *Effect of aerodynamic forces: physical interpretation*

If the discussion reported in Demasi et al. (2013b), Cavallaro et al. (2012) and Cavallaro et al. (2014a) is recalled, the configuration undergoing an instability phenomenon showed a specific deformation pattern, in which the upper wing presented a more pronounced tendency to bend downward, as opposed to the stable cases. Closely inspecting the configurations for the present case (see Fig. 13), it is evident that when aerodynamic forces are acting, the upper wing has a tendency to present an upward bending of the mid-section. Thus, the aerodynamic loads are distributed in such a way to favor this pattern and this is demonstrated in Fig. 14, where the projections (in a variational sense) of aerodynamic forces to the structural nodes are shown. Notice that, for clarity purposes, the forces are not scaled with their actual value.

For low speed/deformations, these loads are distributed almost uniformly, however, for higher speeds they are mainly concentrated on the mid-section of the upper wing, where the bending/torsion increases the local angle of attack.

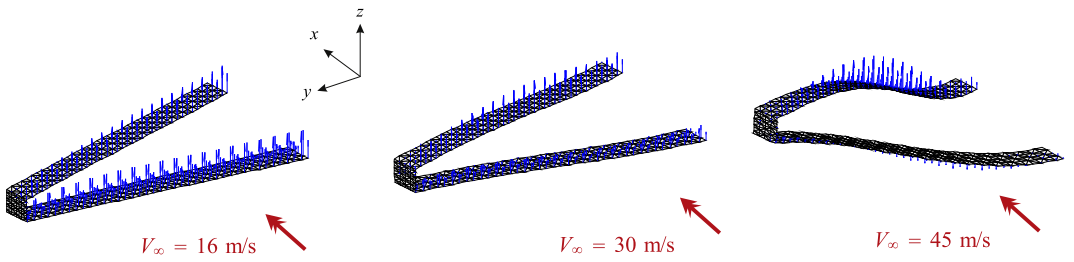

Fig. 14. Deformations at different flow speeds. Also the correspondent aerodynamic load distributions (not scaled) are depicted.

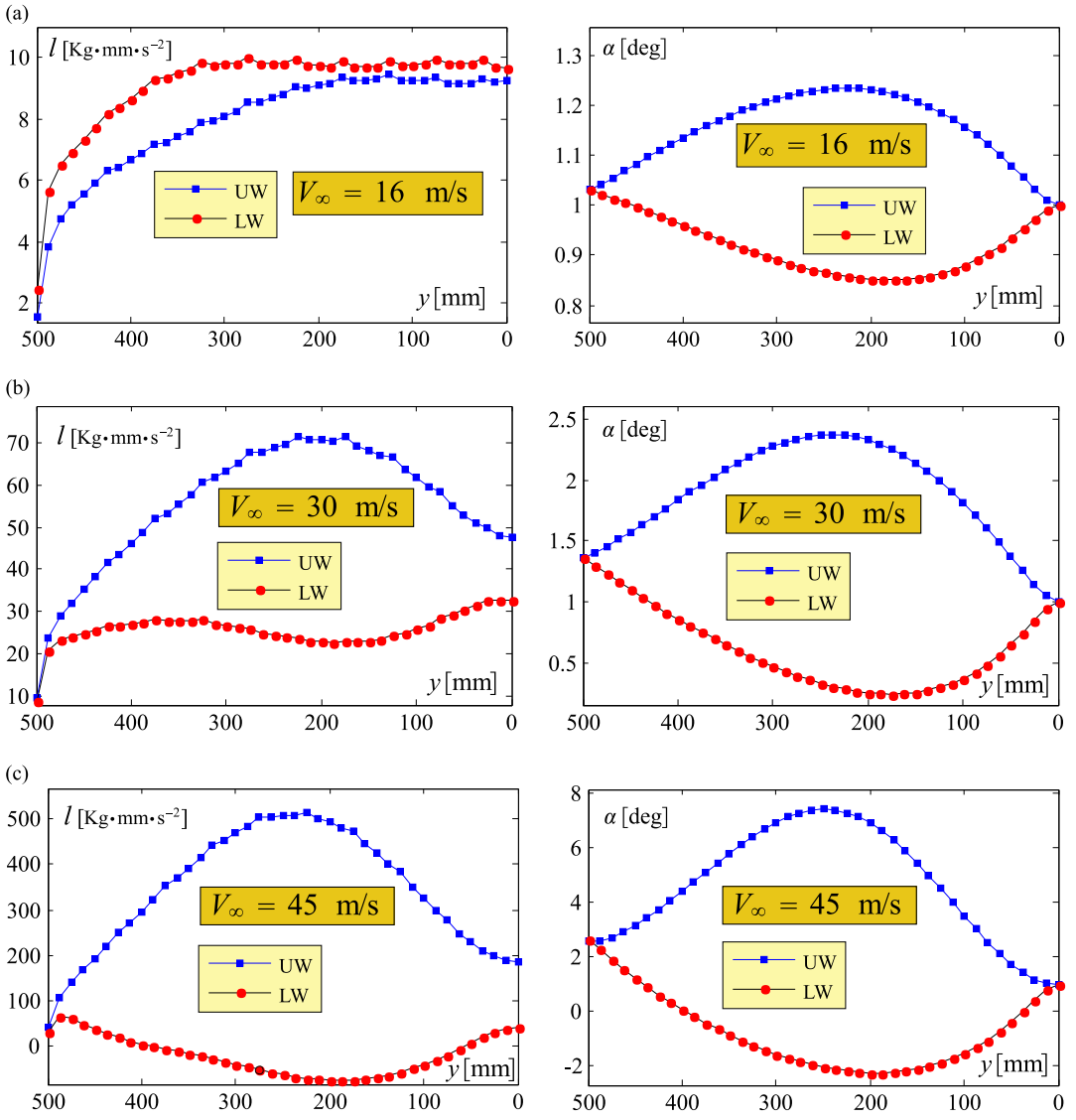

Fig. 15. Sectional lift distribution on the wings. On the right column: geometrical twist of the sections. Results are shown for different flow speeds, as indicated in the figure. All the plots refer to both the upper (UW) and lower wings (LW). (a) Case with $V_\infty = 16$ m/s. (b) Case with $V_\infty = 30$ m/s. (c) Case with $V_\infty = 45$ m/s.

To further investigate the underlying physics, the sectional lifting forces as well as the twist of the sections are depicted in Fig. 15. The initial progressive reduction (increase) in geometrical twist for the lower (upper) wing could be observed due to particular bending–torsion coupling associated with back (forward)-sweep angle of the wing (see Fig. 15(a)). This variation of twist is more pronounced in the mid-span area. The aerodynamic loads are very sensitive to variation in twist,

thus this deformation promotes a progressive reduction (increase) of loads acting on the lower (upper) wing. This effect is even larger than the mutual aerodynamic induction, which actually tends to favor an increase of lift of the lower wing (up-wash) and viceversa, a decrease for the upper wing (down-wash). In fact, in Fig. 15(b) it is clearly shown that the lower wing carries a smaller portion of the overall lifting forces, and undergoes a consistent decrease of the geometric twist angle. For higher speed, e.g. Fig. 15(c), the lower wing could even reach situations of a downforce production (no practical indications on the actual design of Joined Wings is implied on this regard; however this model gives qualitative information on the large increments of loads on the upper wing). Being the twist angle increments concentrated in the mid-span area, the lift distribution for the upper wing is approximately more concentrated in the same region, promoting then the final configuration with the upper wing presenting an upward bending.

For this particular configuration, results suggest that the usage of non-aerodynamic forces in order to study the static structural response of Joined Wings may lead to penalizing results, especially when follower mechanical forces are used.

Before further proceeding, it may be recalled that for the present aerodynamic model the direction of the loads remains fixed with the initial configuration. Thus, the deformations drive a change in the entity of the aerodynamic actions, but not in their direction. That said, a question is still posed on the opportunity to use follower mechanical loading in order to model aerodynamic forces, as it has been common practice. In this regard, a more definitive answer can be given using a higher order aerodynamic solver (see Cavallaro et al., 2014b).

It is indeed true that using mechanical loads has been an appropriate choice in the preliminary steps when exploratory analyses were needed and the instabilities associated with these novel configurations were first brought to light Demasi et al. (2013b), Cavallaro et al. (2012, 2014c): this approach has been crucial not only to understand as much as possible the snap phenomenon from a physical point of view, to predict it, and to understand how to avoid it, but also to reveal possible complex scenarios such as detached static equilibrium branches.

If a more decisive conclusion on the appropriateness of using mechanical loading for experimental purposes is needed, then the distribution of loads over the wings should at least qualitatively resemble the real case. This was discussed in Demasi et al. (2013a, Section VIII, Subsection C), and is here not reported.

8.3. *Effects of bending/torsion coupling and overconstrained nature of Joined Wings: physical interpretation*

Effects of the bending/torsion coupling were tackled in Cavallaro et al. (2012, 2014a) for the case of pure structural loading. With reference to those works, both geometrical (sweep angle) and material (composites) coupling were examined, observing a very strong effect on the stability. Furthermore, in the most complicated cases it was difficult to make any prediction and fully understand the underlying physics. For example, changing fibers direction, and thus acting on the coupling at material level, it was possible to have responses having or not snap-buckling phenomena.

In the presence of aerodynamic forces, there is a very strong dependence on the shape of the configuration, especially on the twist distribution. Thus the overall sensitivity to the deformation is now enhanced. As a consequence, bending/torsion coupling plays a key-role in determining the response.

Traditionally, one of the use of composite materials (aeroelastic tailoring) has aimed to exploit the advantage of this coupling in order to avoid instability phenomena as, for example, aeroelastic divergence. However, when Joined Wings are considered, the situation is more complicated by the overconstrained nature of the system, which opens the door to a new scenario.

In the previous sections it was observed that the coupling due to the geometry (sweep angle) was responsible of a tendency of concentrating the lifting actions in the mid-span region of the upper wing. In fact, a negative (positive) sweep angle promotes an increase (decrease) of twist as consequence of a bending action. Since the system is overconstrained (the wings are joined at the tip) the two different tendencies are mitigated, in the sense that having the twist angle to be approximately the same at the tip (this is true because the joint is small and could be thought as rigid), the relative increase (decrease) of twist is counteracted, especially in that region, see e.g. Fig. 15.

This particular redistribution of twist and loads was thought as being the main *anti-snap* mechanism. To demonstrate it, a particular configuration employing the same geometrical and material properties of *PrP40* but having unswept wings is now studied. Results of the investigation are shown in Fig. 16. The graphs clearly show a snap-divergence occurrence. The analysis completely supports the role played by bending/torsion coupling in preventing snap-divergence through a redistribution of the loads.

Consider now the swept *PrP40* layout, and suppose a more uniform load distribution is sought. One may think to exploit the anisotropic properties of a composite material (coupling at material level). An immediate action would be to design/fine-tune each wing separately. Within this perspective, the coupling introduced through the composite material should ideally counteract the geometric coupling, thus, a positive (negative) coupling is sought for the lower (upper) wing. In other words, to avoid a local decrease in lift on the lower wing, a tendency that favours a positive twist for a bending deformation is needed. And viceversa for the upper one. However, this is where effects of the overconstrained system come into play: the joint transfers the actions, and the wanted/expected result may not be easily achieved.

Summarizing, the importance of structural geometric nonlinearities and the overconstrained nature of the system turns the design in a really challenging one, since actions that may arise spontaneously for addressing a particular issue in a *wanted* direction on a particular wing, may end up creating other unexpected consequences. More investigations on this regard will be presented in future works.

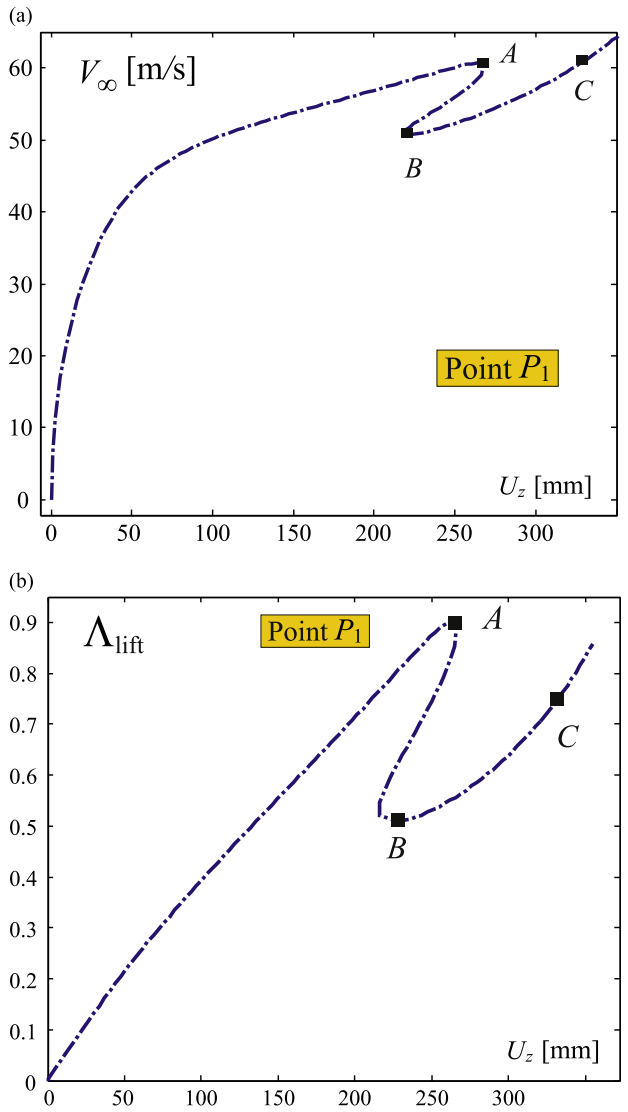

Fig. 16. Flow speed V_∞ (in m/s) versus cumulative vertical displacement U_z (in mm) for lower wing tip point P_1 of the unswept version of joined-wing layout *PrP40*. The flow is directed along the *x*-axis, and the geometry is rotated to 1° in order to create an initial angle of attack. (a) Speed versus vertical displacement of the tip. (b) Lift load level versus speed.

9. Conclusions

In the framework of Joined Wings and for the first time, this work introduced the concept of *snap-divergence* as the condition at which the aeroelastic tangent matrix becomes singular, and compared the results with linearized divergence speeds obtained via eigenvalue analysis.

Two types of Joined Wings were investigated. The first one (named *JW*70) had the joint located at 70% of the wing span. The second one (named *PrP*40) was a PrandtlPlane-like wind tunnel model with the joint located at the tip of the wing.

Numerical analyses showed that *JW*70 experienced snap-divergence. Linearized divergence evaluations, about steady states corresponding to different freestream velocities, were also conducted, showing that for the *JW*70 the eigenvalue approach is not reliable and overestimates the speed at which the instabilities occur (unsafe). The linearized divergence speed was close to the actual snap-divergence speed only for steady states near to the true unstable (snap-divergence) point.

A comparison of the response of the system subjected to aerodynamic, conservative, and follower loads was also carried out for the configuration *JW*70. The response obtained with aerodynamic loads was not showing any abrupt loss in lifting capacity, as it happened for the two mechanical cases (for these last cases this loss in load carrying coincides with the snap condition). Thus, in contrast with what verified above about snap-divergence, one may have erroneously concluded that the aeroelastic response was not associated to any form of instabilities. The conceptual error is that, trying to quantify the static

deflections to an applied load, aeroelastic instabilities cannot be taken into account. Thus, mimicking aeroelastic loads with mechanical forces should be carefully meditated upon.

The second analyzed joined-wing configuration, the *PrP*40, did not experience snap-divergence. However, from the system's response it was possible to notice a softening followed by a stiffening without a true mathematical snap-divergence occurrence. The corresponding linearized divergence, obtained with an eigenvalue approach, showed its minimum value at the end of the softening region.

Aerodynamic load distributions due to the aeroelastic deformation promoted an upward bending of the upper wing, a pattern that was noticed in Demasi et al. (2013b) and Cavallaro et al. (2012) for PrandtlPlane-like configurations not incurring in buckling instability. This last example demonstrated that the overconstrained and nonlinear response of a Joined Wing can also have positive effects on the stability properties, if properly understood. This cannot be conclusive because of the simplified wind tunnel-like models presented in the study and the focus on static analysis. But the study gave indications on what the challenges and opportunities that these joined-wing configurations represent.

References

Blair, M., Canfield, R.A., Roberts Jr., R.W., 2005. Joined-wing aeroelastic design with geometric nonlinearity. Journal of Aircraft 42 (July (4)), 832–848.

Bond, V., Canfield, R.A., Cooper, E.J., Blair, M., 2012. Experimental nonlinear static deflection of a subscale joined wing. Journal of Aircraft 49 (January–February (1)), 329–333. URL: ⟨http://arc.aiaa.org/doi/abs/10.2514/1.C031423⟩.

Boston, J., Swenson, E., Kunz, D., 2010. Experiments with geometric non-linear coupling for analytical validation. In: Presented at the 51st AIAA/ASME/ASCE/AHS/ASC Structures, Structural Dynamics and Materials Conference, Orlando, Florida, 12–15 April 2010.

Cavallaro, R., Demasi, L., Passariello, A., 2012. Nonlinear analysis of PrandtlPlane Joined Wings. Part II. Effects of anisotropy. No. AIAA 2012-1462. In: 53rd AIAA/ASME/ASCE/AHS/ASC Structures, Structural Dynamics, and Materials Conference, Honolulu, Hawaii, 23–26 April 2012. URL: ⟨http://arc.aiaa.org/doi/abs/10.2514/6.2012-1462⟩.

Cavallaro, R., Demasi, L., Passariello, A., 2014a. Nonlinear analysis of prandtl plane joined wings: effects of anisotropy. AIAA Journal 52 (5), 964–980. 10.2514/1.J052242.

Cavallaro, R., Iannelli, A., Demasi, L., Razon, A., 2014b. Phenomenology of nonlinear aeroelastic responses of highly deformable joined-wings configurations. No. AIAA 2014-1199. In: 55th AIAA/ASMe/ASCE/AHS/SC Structures, Structural Dynamics, and Materials Conference, AIAA Science and Technology Forum and Exposition (SciTech2014) National Harbor, Maryland, 13–17 January 2014. URL: ⟨http://arc.aiaa.org/doi/abs/10.2514/6.2014-1199⟩.

Cavallaro, R., Demasi, L., Bertuccelli, F., Benson. D.J., 2014c. Risks of linear design of joined wings: a non-linear dynamic perspective in the presence of follower forces. CEAS Aeronaut J, ⟨http://dx.doi.org/10.1007/s13272-014-0136-x⟩.

Chambers, J.R., November 2005. Innovation in flight: research of the NASA Langley research center on revolutionary advanced concepts for Aeronautics. No. 39 in Monograph in Aerospace History. NASA, NASA SP 2005-4539.

Crisfield, M., 1991. Non Linear Finite Element Analysis of Solid and Structures, vol. 1. John Wiley & Sons, New York.

Demasi, L., Cavallaro, R., Bertuccelli, F., 8-11 April 2013a. Post-critical analysis of Joined Wings: the concept of snap-divergence as a characterization of the instability. No. AIAA 2013-1559. 54th AIAA/ASME/ASCE/AHS/ASC Structures, Structural Dynamics, and Materials Conference, Boston, Massachusetts, American Institute of Aeronautics and Astronautics. URL: ⟨http://arc.aiaa.org/doi/abs/10.2514/6.2013-1559⟩.

Demasi, L., Cavallaro, R., Razon, A., 2013b. Post-critical analysis of PrandtlPlane joined-wing configurations. AIAA Journal 51 (1), 161–177.

Demasi, L., Livne, E., 2005. Exploratory studies of joined wing aeroelasticity. In: Presented at the 46th AIAA/ASME/ASCE/AHS/ASC Structures, Structural Dynamics and Materials Conference, Austin, Texas, 18–21 April 2005. URL: ⟨http://arc.aiaa.org/doi/abs/10.2514/6.2005-2172⟩.

Demasi, L., Livne, E., 2007. The Structural Order reduction challenge in the case of geometrically nonlinear joined-wing configurations. In: Presented at the 48th AIAA/ASME/ASCE/AHS/ASC Structures, Structural Dynamics and Materials Conference, Honolulu, Hawaii, 23–26 April 2007.

Demasi, L., Livne, E., 2009a. Aeroelastic coupling of geometrically nonlinear structures and linear unsteady aerodynamics: two formulations. Journal of Fluids and Structures 25, 5. URL: ⟨http://www.sciencedirect.com/science/article/pii/S0889974609000395⟩.

Demasi, L., Livne, E., 2009b. Contributions to joined-wing aeroelasticity. In: Presented at the International Forum on Aeroelasticity and Structural Dynamics Conference, Seattle, Washington, 21–25 June 2009.

Demasi, L., Livne, E., 2009c. Dynamic aeroelasticity of structurally nonlinear configurations using linear modally reduced aerodynamic generalized forces. AIAA Journal 47, 71–90.

Demasi, L., Palacios, A., 2010. A reduced order nonlinear aeroelastic analysis of joined wings based on the proper orthogonal decomposition. In: Presented at the 51st AIAA/ASME/ASCE/AHS/ASC Structures, Structural Dynamics & Materials Conference, Orlando, Florida, 12–15 April 2010.

Dowell, E., Edwards, J., Strganac, T., 2003. Nonlinear aeroelasticity. Journal of Aircraft 40 (September (5)), 857–874. URL: ⟨http://dx.doi.org/10.2514/2.6876⟩.

Frediani, A., 1999. Large Dimension Aircraft US Patent 5,899,409.

Frediani, A., 2002. New large aircraftEuropean Patent EP 0716978B1, 20 March 2002.

Frediani, A., 2003. Velivolo biplano ad ali contrapposteItalian Patent FI 2003A000043, 19 February 2003.

Frediani, A., June 2005. The prandtl wing. In: Innovative Configurations and Advanced Concepts for Future Civil Aircraft. VKI Lecture Series 2005–2006, p. 661. Von Karman Institute. ISBN: 2-930389-62-1.

Frediani, A., Cipolla, V., Rizzo, E., 2012. The PrandtlPlane configuration: overview on possible applications to civil aviation. In: Buttazzo, G., Frediani, A. (Eds.), Variational Analysis and Aerospace Engineering: Mathematical Challenges for Aerospace Design Springer Optimization and Its Applications, vol. 66. , Springer, US, pp. 179–210. URL: ⟨http://dx.doi.org/10.1007/978-1-4614-2435-2_8⟩.

Heeg, J., Morelli, E., 2011. Evaluation of simultaneous-multisine excitation of the joined wing sensorcraft aeroelastic wind tunnel model. In: Presented at the 52nd AIAA/ASME/ASCE/AHS/ASC Structures, Structural Dynamics & Materials Conference, Denver, Colorado, 4–7 April 2011.

Katz, J., Plotkin, A., 2001. In: Low-Speed Aerodynamics. Cambridge Aerospace SeriesCambridge University Press, New York. URL: ⟨http://books.google.com/books?id=rAS1DmBRLo8C⟩.

Kim, T., Swenson, E., Kunz, D., Lindsley, N., Blair, M., 2011. Follower-force experiments with geometric nonlinear coupling for analytical validation. No. AIAA 2011-1978. In: 52nd AIAA/ASME/ASCE/AHS/ASC Structures, Structural Dynamics, and Materials Conference, Denver, Colorado, 4–7 April 2011.

Kim, Y.I., Park, G.J., Kolonay, R.M., Blair, M., Canfield, R.A., 2008. Nonlinear response structural optimization of a joined wing using equivalent loads. AIAA Journal 46.

Levy, R., Spillers, W., 2003. Analysis of Geometrically Nonlinear Structures. No. v. 1. Kluwer Academic Publishers, Dordrecht, Netherlands.

Liu, S., Wickert, D.P., Canfield, R.A., 2010. Fluid-structure transient Gust response sensitivity for a nonlinear joined wing model. In: Presented at the 51st AIAA/ASME/ASCE/AHS/ASC Structures, Structural Dynamics and Materials Conference, Orlando, Florida, 12–15 April 2010.

Patil, M.J., 2003. Nonlinear aeroelastic analysis of joined-wing aircraft. In: Presented at the 44th AIAA/ASME/ASCE/AHS/ASC Structures, Structural Dynamics and Materials Conference, Norfolk, Virginia, April 7–10, 2003.

Phlipot, G., Wang, X., Mignolet, M., Demasi, L., Cavallaro, R., 2014. Nonintrusive reduced order modeling for the nonlinear geometric response of some joined wings. No. AIAA 2014-0151. In: 55th AIAA/ASMe/ASCE/AHS/SC Structures, Structural Dynamics, and Materials Conference, AIAA Science and

Technology Forum and Exposition (SciTech2014) National Harbor, Maryland, American Institute of Aeronautics and Astronautics, 13–17 January 2014. URL: ⟨http://arc.aiaa.org/doi/abs/10.2514/6.2014-0151⟩.
Rankin, C., Nour-Omid, B., 1988. The use of projectors to improve finite element performance. Computers and Structures 30 (1–2), 257–267. URL: ⟨http://www.sciencedirect.com/science/article/pii/0045794988902313⟩.
Reichenbach, E., Castelluccio, M.B.S., 2011. Joined wing sensorcraft aeroservoelastic wind tunnel test program. In: Presented at the 52nd AIAA/ASME/ASCE/AHS/ASC Structures, Structural Dynamics and Materials Conference, Denver, Colorado, 4–7 April 2011.
Riks, E., 1979. An incremental approach to the solution of snapping and buckling problems. International Journal of Solids and Structures 15 (7), 529–551. URL: ⟨http://www.sciencedirect.com/science/article/pii/0020768379900817⟩.
Rodden, W.P., Johnson, E.H., 1994. User Guide V 68 MSC/NASTRAN Aeroelastic Analysis. MacNeal-Schwendler Corporation.
Scott, M., Enke, A., Flanagan, J., 2011. Sensorcraft free-flying aeroservoelastic model design and fabrication. In: Presented at the 52nd AIAA/ASME/ASCE/AHS/ASC Structures, Structural Dynamics and Materials Conference, Denver, Colorado, 4–7 April 2011.
Sotoudeh, Z., Hodges, D.H., 2011. Incremental method for structural analysis of joined-wing aircraft. Journal of Aircraft 48 (September (5)), 1588–1601.
Teunisse, N., Tiso, P., Demasi, L., Cavallaro, R., 2014. A computational method for structurally nonlinear joined wings based on modal derivatives. No. AIAA 2014-0494. In: 55th AIAA/ASMe/ASCE/AHS/SC Structures, Structural Dynamics, and Materials Conference, AIAA Science and Technology Forum and Exposition (SciTech2014) National Harbor, Maryland, American Institute of Aeronautics and Astronautics, 13–17 January 2014. URL: ⟨http://arc.aiaa.org/doi/abs/10.2514/6.2014-0494⟩.
Weisshaar, T.A., Lee, D.H., 2002. Aeroelastic tailoring of joined-wing configurations. In: 43nd AIAA/ASME/ASCE/AHS/ASC Structures, Structural Dynamics and Materials Conference, Denver, CO, 22–25 April 2002.
Wolkovitch, J., 1986. The joined wing aircraft: an overview. Journal of Aircraft 23 (March (3)), 161–178.
ZONA Technology Inc., 2004. ZAERO. Theoretical Manual, Version 7.1.